Pergamon

Int. J. Heat Mass Transfer. Vol. 40, No. 11, pp. 2679–2690, 1997

Printed in Great Britain
0017–9310/97 $17.00+0.00

PII: S0017–9310(96)00275–X

Experimental study of transient natural convection in an inclined rectangular enclosure

T. D. UPTON and D. W. WATT

Department of Mechanical Engineering, University of New Hampshire, Durham, NH 03824, U.S.A.

(*Received* 12 *February* 1996 *and in final form* 29 *July* 1996)

Abstract—Simultaneous quantitative measurements are made of both the temperature and velocity fields for two-dimensional transient natural convection in an inclined rectangular enclosure using calibrated multichannel electronic interferometry and digital particle image velocimetry. The transient boundary conditions are initiated impulsively by heating and cooling two opposing walls. The evolution of the flow to steady-state is determined for a Prandtl number of 6.38, a Rayleigh number of 1.5×10^5 and an aspect ratio of 1.0, at angles of inclination of $\pi/4$, $\pi/2$ and $3\pi/4$. © 1997 Elsevier Science Ltd. All rights reserved.

1. INTRODUCTION

Transient natural convection in enclosures in which the temperatures of two opposing walls are initiated impulsively has been the focus of a number of experimental and numerical investigations. In the enclosures of interest, convection boundary layers form on the heated and cooled walls. The boundary layers are redirected by the other two walls of the enclosure and flow across the enclosure as intrusion layers. Previous numerical results have indicated that transient oscillations consisting of two distinct boundary oscillations and a whole cavity oscillation occur during the initial stages of the flow. Several of the experimental studies confirm the existence of the two boundary layer oscillations, but none has shown the whole cavity oscillations. The present work is an effort to confirm the existence of all the transient oscillations experimentally.

Natural convection in inclined enclosures has also been studied using experimental and numerical methods. The angle of inclination has been shown to have a pronounced effect on the flow structure. In the present work, scale analysis is used to determine the important terms in the equations of motion as a function of the angle of inclination and to produce estimates of the time and length scales for the boundary layers and intrusion layers.

In the present work, simultaneous quantitative measurements are made of both the temperature and velocity fields for two-dimensional transient natural convection in an inclined rectangular enclosure (Fig. 1). The fluid in the enclosure is initially stationary and isothermal. The transient boundary conditions are initiated impulsively by heating and cooling two opposing walls. The other two walls are insulated and nonconducting. The temperature is measured using calibrated multichannel electronic interferometry (CMEI), and the velocity is measured using digital particle image velocimetry (DPIV).

2. PREVIOUS WORK

At high Rayleigh numbers the flow exhibits oscillatory behavior which depends on the boundary conditions. Transient oscillations occurring at startup and nondecaying periodic oscillations have been observed. Transient oscillations have been observed in enclosures consisting of two isothermal vertical walls and two insulated and nonconducting horizontal walls, while periodic oscillations have been observed in enclosures consisting of two isothermal vertical walls and two conducting horizontal walls in which a linear temperature gradient exists between the two isothermal vertical walls. A discussion of both transient and periodic oscillations is included for completeness and because nonideal experimental boundary conditions may lead to both types.

Patterson and Imberger [1] claimed the transient oscillations resulted because the entrainment length of the vertical boundary layers is greater than the thickness of the horizontal intrusion layers; as the discharged intrusion layers reach the vertical boundary layers, they spread against buoyancy to meet the entrainment length, tilting the isotherms beyond the horizontal and generating internal waves. In an experimental study Ivey [2] did not see any evidence of regular cavity scale internal waves. He argued instead that the transient oscillations occurred because of an internal hydraulic jump with an increase in thickness of the horizontal intrusion layers as they emerge from the vertical boundary layers. The transient oscillations were stated to disappear as the interior is set in motion and stratifies in temperature, increasing the thickness

NOMENCLATURE

A	aspect ratio
f	frequency
$\bar{h}$	average convection heat transfer coefficient
H	height of the isothermal vertical walls
n	refractive index
Pr	Prandtl number
q	rate of heat transfer
Ra	Rayleigh number
Ra_c	critical Rayleigh number
T_v	time for a viscous intrusion layer to travel across the enclosure
ΔT	temperture difference
v	thermal boundary layer velocity
W	width of the adiabatic horizontal walls
x_w	wall thickness
z_p	path length through the phase object.

Greek symbols

α	thermal diffusivity
γ	angle of inclination
δ_T	thermal boundary layer thickness
δ_v	velocity boundary layer thickness
Δ_v	viscous intrusion layer thickness
λ	wavelength of the light
ν	kinematic viscosity
τ	thermal boundary layer growth time
τ_c	conduction time
T	period
ω	angular frequency
Ω	generalized frequency.

Subscripts

0	initial.

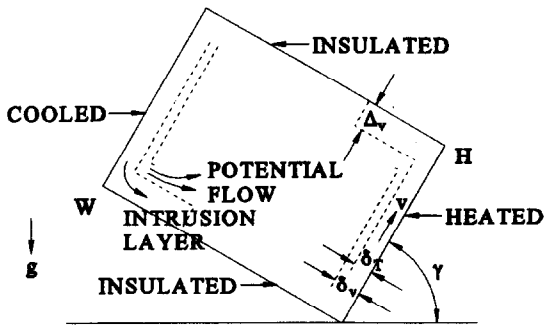

Fig. 1. Schematic of an inclined rectangular enclosure showing two-layer flow structure.

of the intrusion and flooding the hydraulic jump. In a direct numerical simulation Schladow [3] found transient oscillations consisting of two distinct boundary layer instabilities and a whole cavity oscillation. The first of the boundary layer instabilities was attributed to the leading edge effect of the vertical boundary layer. The second was attributed to the impact of the horizontal intrusion from the opposing vertical wall with the boundary layer. The frequency of these oscillations was determined by selective amplification of the disturbance and was higher than the frequency of the whole cavity oscillations. The whole cavity oscillations were attributed to the horizontal pressure gradient established by changes in the intrusion temperature field. These whole cavity oscillations were stated as determining the nature of the flow in the interior as the oscillation produces a flow in the opposite direction of the intrusion flow. The internal hydraulic jump proposed by Ivey [2] was shown instead to be a complex recirculation zone. In an experimental and numerical investigation Patterson and Armfield [4] came to similar conclusions. The two boundary layer oscillations were attributed to travelling wave instabilities on the boundary layer caused first by initiation of the boundary layer and second by impact of the incoming intrusion. The whole cavity oscillations were stated to result from the splitting of the horizontal intrusion as it impacts the opposite wall. Armfield and Patterson [5] stated that the first boundary layer instability takes the form of waves travelling in the flow direction caused by the initial singularity generated at the leading edge of the boundary layer. Temperature overshoot is possible if the temperature at a point rises to a higher value than at steady state before the leading edge arrives. They agreed that the boundary layer selectively amplifies a single wavenumber.

Briggs and Jones [6] claimed the periodic oscillations are induced by the linear horizontal surface temperature. They stated that the vertical temperature gradient in the horizontal intrusions is unstable, since the hot intrusion is cooled from the top and the cold intrusion is heated from the bottom as they cross the enclosure. They hypothesized that the periodic oscillations are a resonance phenomena between travelling waves along the top and bottom of the enclosure and the natural buoyant frequency of the stratified fluid in the interior of the enclosure. Winters [7] showed that the periodic oscillations arise as a Hopf bifurcation, and agreed with Briggs and Jones [6] that the oscillations are the result of a resonance phenomena between the travelling waves and gravity waves in the stratified interior of the enclosure.

By use of linear stability analysis, Gebhart and Mahajan [8] determined that the frequency of the boundary layer transient oscillations is

$$\omega = \frac{\nu Ra^{2/3}\Omega}{H^2 Pr^{2/3}}, \tag{1}$$

where ν is the kinematic viscosity, Ra is the Rayleigh number, Ω is a generalized frequency, H is the height of the isothermal vertical walls and Pr is the Prandtl number. By use of scale analysis, Patterson and Imberger [1] showed that the frequency of the whole cavity transient oscillations is

$$\omega \sim \frac{\sqrt{\nu\alpha Ra}}{H^2\sqrt{1+A^2}}, \tag{2}$$

where α is the thermal diffusivity and A is the aspect ratio defined by

$$A = \frac{H}{W}, \tag{3}$$

where W is the width of the adiabatic horizontal walls. Gebhart and Mahajan [8] reproduced stability planes which show contours of constant amplification rate for vertical walls dissipating a uniform heat flux and give the critical Rayleigh number for boundary layer transient oscillations. Hieber and Gebhart [9] gave equations relating walls dissipating a uniform heat flux to isothermal walls. Patterson and Imberger [1] showed that the critical Rayleigh number for whole cavity transient oscillations is

$$Ra_c \sim Pr^4 A^{-4}. \tag{4}$$

3. SCALE ANALYSIS

The scale analysis discussed here follows the scaling arguments Patterson and Imberger [1] made for an enclosure with $\gamma = \pi/2$, where γ is the angle of inclination defined by the angle of the heated wall from the horizontal direction (Fig. 1). This scale analysis is based on the assumption that both the boundary layers and the intrusion layers are distinct. At times larger than the thermal boundary layer growth time τ, the fluid near the heated and cooled walls is characterized by a two-layer structure consisting of an inner thermal boundary layer of thickness δ_T and an outer wall jet of thickness δ_v shown in Fig. 1 [1, 10]. The heated fluid from the thermal boundary layer crosses the enclosure in an intrusion layer, while the unheated fluid from the wall jet discharges as a potential flow into the interior of the enclosure [1, 10].

The fluid in the enclosure is modeled as Newtonian, incompressible, and constant property. The Boussinesq approximation is used in the Navier–Stokes equations. The thermal boundary layer grows until the heat conducted through the wall is balanced by that convected away by the buoyant layer [1, 10]. For a fluid with $Pr \geqslant 1$ the thickness scale for the thermal boundary layer is

$$\delta_T \sim \frac{H}{[\sin(\gamma)Ra]^{1/4}}, \tag{5}$$

the growth time scale is

$$\tau \sim \frac{H^2}{\alpha[\sin(\gamma)Ra]^{1/2}}, \tag{6}$$

and the velocity scale is

$$v \sim \frac{\alpha[\sin(\gamma)Ra]^{1/2}}{H}, \tag{7}$$

based on an energy balance between convection and conduction. The diffusion of momentum out of the thermal boundary layer maintains an outer velocity boundary layer in which the effect of buoyancy is minor [1, 10]. The thickness scale for the velocity boundary layer is

$$\delta_v \sim \frac{HPr^{1/2}}{[\sin(\gamma)Ra]^{1/4}}, \tag{8}$$

based on a momentum balance between inertia and viscous diffusion.

If $\gamma \sim \pi/2$ the intrusion layer is dominated by pressure resulting from buoyancy in the boundary layer and the thickness scale for a viscous intrusion layer is [1]

$$\Delta_v \sim \frac{H^{3/4}W^{1/4}}{Ra^{3/16}}, \tag{9}$$

and the time scale for the intrusion layer to travel across the enclosure is [1]

$$T_v \sim \frac{H^{3/4}W^{5/4}}{\alpha Ra^{7/16}}, \tag{10}$$

based on a momentum balance between boundary layer buoyancy and viscous diffusion. If $\gamma \nsim \pi/2$ the intrusion layer is dominated by buoyancy in the intrusion layer itself, and the thickness scale for a viscous intrusion layer is

$$\Delta_v \sim \frac{H[\sin(\gamma)]^{1/12}}{[\cos(\gamma)]^{1/3}Ra^{1/4}}, \tag{11}$$

and the time scale for the intrusion layer to travel across the enclosure is

$$T_v \sim \frac{HW}{\alpha[\sin(\gamma)]^{1/6}[\cos(\gamma)]^{1/3}Ra^{1/2}}, \tag{12}$$

based on a momentum balance between intrusion layer buoyancy and viscous diffusion.

4. EXPERIMENTAL APPARATUS AND PROCEDURE

Simultaneous quantitative measurements were made of both the temperature and velocity fields using CMEI and DPIV. The evolution of the flow to steady-state was determined for $Pr = 6.38$, $Ra = 1.5 \times 10^5$ and $A = 1.0$, at $\gamma = \pi/4$, $\gamma = \pi/2$ and $\gamma = 3\pi/4$. The technique of CMEI is introduced by Upton and Watt [11], and design considerations are detailed by Upton and Watt [12]. The technique of DPIV is discussed

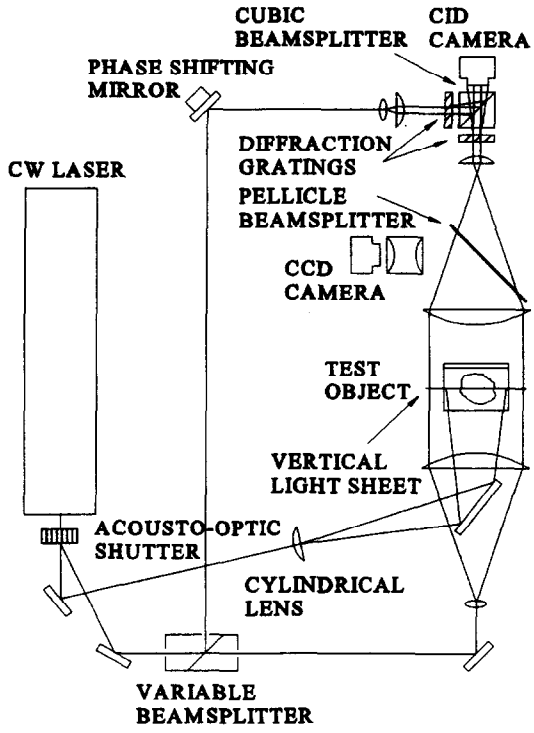

Fig. 2. Schematic of the simultaneous implementation of a calibrated multichannel electronic interferometer and a digital particle image velocimeter.

by Willert and Gharib [13]. CMEI and DPIV were implemented simultaneously using the combined optical setup shown in Fig. 2.

The experiments were performed in a rectangular enclosure measuring 3.0 cm wide × 3.0 cm high × 6.0 cm long consisting of two isothermal walls and two insulated and nonconducting walls (Fig. 3). The enclosure was constructed from acrylic glass 5.4 mm thick. The two isothermal walls were made from 0.30 mm thick experimental grade copper. The two walls in the interferometer path were 12.7 mm thick optical windows made from BK-7. The seal between the optical windows and the enclosure was made using rubber o-rings and an adjustable clamp system. The enclosure was filled with water seeded with particles. The optical windows and the adjustable clamp system were necessary to eliminate refraction in the phase object path as the light passed through the interfaces between the air, water and windows. The particles used were Bangs Laboratories Incorporated P0750000PN macro beads made from styrene and paramethylstyrene. They had a density of 1.020×10^3 kg m^{-3} and a diameter range of 50–90 μm with an average diameter of 75.000 μm. To make the particles neutrally buoyant, sodium bicarbonate was added to the water in the enclosure until its density was 1.02×10^3 kg m^{-3}.

NESLAB Instruments Incorporated EX-111D and RTE-111D temperature controlled baths with water as the working fluid were used to control the temperature of the two isothermal walls. The temperature stability of the baths was specified as ± 0.01°C. The EX-111D bath was maintained at $T_0 + \Delta T$, while the RTE-111D bath was maintained at $T_0 - \Delta T$. The magnitude of ΔT was limited due to refraction errors. In order for the deviation due to refraction to be less than $\lambda/10$ [14],

$$\frac{\left(\frac{dn}{dy}\right)^2 z_p^3}{n(y)\lambda_0} < 0.3, \tag{13}$$

where dn/dy is the refractive index gradient, z_p is the path length through the phase object, $n(y)$ is the refractive index, and λ_0 is the wavelength of the light. The maximum temperature gradient is then given by

$$\frac{dT}{dy} < \sqrt{0.3 \frac{n(y)\lambda_0}{\left(\frac{dn}{dT}\right)^2 z_p^3}}, \tag{14}$$

where dn/dT is the change in the refractive index with temperature. For a linear temperature gradient, the temperature difference is limited to

$$\Delta T < \left[\frac{\nu \alpha H}{g\beta \sin(\gamma)}\right]^{1/5} \left[0.3 \frac{n(y)\lambda_0}{\left(\frac{dn}{dT}\right)^2 z_p^3}\right]^{2/5} \tag{15}$$

using equations (5) and (14). For an enclosure with $\gamma = \pi/2$ the temperature difference is limited to $\Delta T < 0.47$°C. The circulation to the two isothermal walls was controlled using two ASCO 8320G178 three way solenoid valves with an operating voltage of 24 V DC. The solenoid valves were located near the enclosure and the bath fluid was circulated through the valves while deenergized to bring the plumbing to the bath temperature. The solenoid valves were controlled by a MetraByte Corporation Dascon-1 digital-analog expansion board. The ambient temperature and the initial temperature of the fluid in the enclosure was approximately $T_0 = 24$°C. To satisfy the condition of equation (15), the temperature difference was $\Delta T = 0.30$°C.

To obtain accurate transient results, it is important that the initiation time of the experiment be small compared to the growth time scale of the thermal boundary layer [4]. The growth time scale for the thermal boundary layer is $\tau \sim 16$ s using equation (6). To initiate the transient boundary conditions, the solenoids were energized, and water from the temperature controlled baths was pumped to the two isothermal walls at a volume flow rate of 1.7×10^{-5} m^3 s^{-1}. At this flow rate the space next to the walls was filled in 0.3 s. The time for the walls to reach 0.9 ΔT was found to be 1.7 s using lumped heat capacity analysis and a convection coefficient of 1.4×10^3 W m^{-2} K^{-1}. This resulted in an initiation time of 2.0 s. Previous experimental studies [2, 4] based the

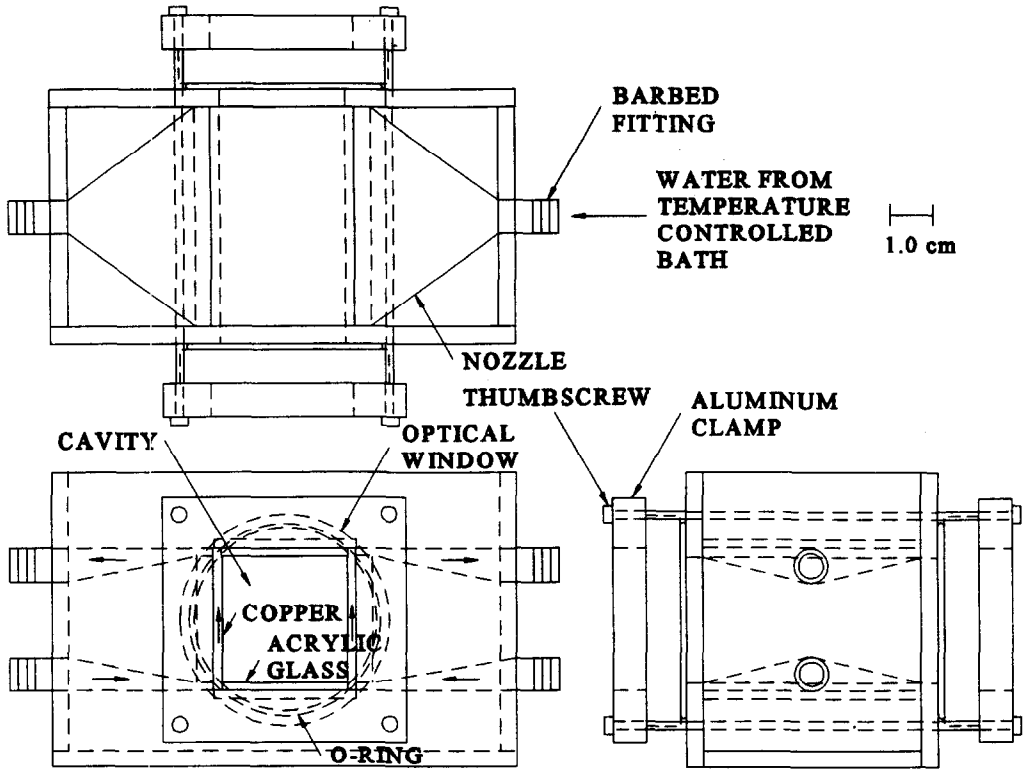

Fig. 3. Schematic of the natural convection enclosure.

initiation time on the conduction time scale through the walls, which is given by

$$\tau_c \sim \frac{x_w^2}{\alpha}, \tag{16}$$

where x_w is the wall thickness. This time scale does not correctly describe the time required for the isothermal walls to change by ΔT.

5. ANALYSIS

Gebhart and Mahajan [8] reported that for $Pr = 6.38$ a generalized frequency of $\Omega = 0.28$ has the highest amplification rate. By use of this value in equation (1), the frequency of the two boundary layer transient oscillations is $f = 0.037$ Hz. The frequency of the whole cavity transient oscillations is $f \sim 0.018$ Hz using equation (2). The frame rate used of 2.5 Hz was high enough to resolve both the boundary layer oscillations and the whole cavity oscillations. Gebhart and Mahajan [8] reported that for $Pr = 6.7$ and $Ra = 1.5 \times 10^5$ the boundary layer flow is in a region of neutral stability; the Rayleigh number is less than that required for amplification of the boundary layer disturbances. The equations of Hieber and Gebhart [9] were used to relate walls dissipating a uniform heat flux to isothermal walls. The critical Rayleigh number for whole cavity transient oscillations is $Ra_c \sim 2 \times 10^3$ using equation (4). Therefore only whole cavity transient oscillations are expected.

Four different quantities have been used to indicate the two boundary layer oscillations. These are the temperature in the boundary layer, the velocity in the boundary layer, the Nusselt number at the wall of the enclosure, and the Nusselt number at the center of the enclosure, all functions of time [2–5]. Of these four quantities, the whole cavity oscillations have been apparent only in Nusselt number at the center of the enclosure [1, 3, 4].

The Nusselt number is defined by

$$Nu = \frac{\bar{h}W}{k}, \tag{17}$$

where $\bar{h}$ is the average convection heat transfer coefficient defined by

$$\bar{h} = \frac{q}{2H\Delta T}, \tag{18}$$

where q is the rate of heat transfer. By use of equations (17) and (18) the Nusselt number at the wall of enclosure is written as [1, 3]

$$Nu_w = \frac{1}{2kA\Delta T}\int_0^H \left(-k\frac{\partial T}{\partial x}\right)\mathrm{d}y, \tag{19}$$

and the Nusselt number at the center of the enclosure is written as [1, 3]

$$Nu_c = \frac{1}{2kA\Delta T}\int_0^H \left(\rho CuT - k\frac{\partial T}{\partial x}\right)\mathrm{d}y. \tag{20}$$

The Nusselt number at the wall and the center of the enclosure are determined from the experimental data using numerical integration.

The temperature and temperature gradient are determined using the method of least squares, resulting in an uncertainty in the temperature field of $\pm 0.002^{\circ}C$ and an uncertainty in the temperature gradient of $\pm 0.002^{\circ}C\ mm^{-1}$. The velocity field is determined to 0.5 pixel accuracy, resulting in an uncertainty in the velocity field of typically ± 0.06 mm/s. The uncertainty in the Nusselt number measurement at the wall is ± 0.02 using equation (19) and the uncertainty in the Nusselt number measurement at the center is ± 0.6 using equation (20). The uncertainty analysis discussed here follows the method described by Holman [15]. A more detailed discussion of data analysis and uncertainty analysis is discussed in Upton [16].

6. RESULTS AND DISCUSSION

The temperature and velocity fields during the evolution of the flow to steady-state are shown for $\gamma = \pi/4$ in Fig. 4, $\gamma = \pi/2$ in Fig. 5, and $\gamma = 3\pi/4$ in Fig. 6. The temperature fields are shown as grey scale maps and the velocity fields are shown by vectors whose length is proportional to the velocity. The absence of temperature data in Figs. 4 and 6 results from the limited usable camera area. Locations where no velocity vectors exist indicate either a velocity of 0 or an absence of data.

Figures 4–6 exhibit differences due entirely to the angle of inclination. Immediately after the transient boundary conditions are initiated, there is no fluid motion and the thermal boundary layer grows by pure conduction, so that initially the temperature and velocity fields are independent of the angle of inclination. This is illustrated at 10 s from startup in Figs. 4(a), 5(a), and 6(a). As the thermal boundary layer continues to grow, it is accelerated by the tangential component relative to the wall of the buoyancy force. Since the normal component relative to the wall of the buoyancy force does not significantly affect the flow for $\pi/6 < \gamma < 5\pi/6$ [10], the temperature and velocity fields for the three angles of inclination are nearly identical and differ only in the apparent Rayleigh number. At 22 s the boundary layer has started to convect as shown in Figs. 4(b), 5(b), and 6(b).

Once the intrusion layer starts to cross the enclosure, the angle of inclination has a more pronounced effect. This is shown at 40 s in Figs. 4(c), 5(c) and 6(c). When $\gamma = \pi/4$, the intrusion layer is drawn across the enclosure as a buoyant jet. Since buoyancy acts along both the heated and insulated walls, there is more work done on the fluid by buoyancy, increasing the velocity. When $\gamma = \pi/2$, the intrusion layer is pushed across by the pressure force due to buoyancy in the boundary layer. When $\gamma = 3\pi/4$, buoyancy and pressure oppose each other in the intrusion layer, decreasing the velocity. By 75 s the intrusion layer is well developed. When $\gamma = \pi/4$, buoyancy draws the heated fluid completely across the enclosure as shown in Fig. 4(d). When $\gamma = \pi/2$ or $\gamma = 3\pi/4$, some of the fluid leaving the boundary layer does not cross the enclosure but instead is entrained back into the boundary layer as shown in Figs. 5(d) and 6(d). The amount of this entrainment depends on the angle of inclination and is larger for $\gamma = 3\pi/4$. Kuyper *et al.* [17] stated that for $\gamma \sim \pi$ most of the fluid leaving the heated or cooled wall returns to the same wall, forming a stretched cell along both walls. When $\gamma = \pi/2$ or $\gamma = 3\pi/4$, the interior of the enclosure is filled by horizontal layering followed by the establishment of a primarily vertical temperature gradient as noted by Patterson and Imberger [1].

The steady-state temperature and velocity fields are shown in Figs. 4(e), 5(e) and 6(e). When $\gamma = \pi/4$, the interior of the enclosure is well mixed and the temperature gradients are small. The current results are consistent with the results of Hamady *et al.* [18] and Kuyper *et al.* [17] who showed for similar angles of inclination a single convection cell. Kuyper *et al.* [17] stated that the flow in the interior of the enclosure pushes the flow along the adiabatic walls to the side, breaking up the temperature stratification. When $\gamma = \pi/2$, a stably stratified vertical temperature gradient exists in the interior of the enclosure. The flow is dominated by a single convection cell, with the primary flow parallel to the isotherms. However, a smaller cell exists near each of the heated and cooled boundaries. The current results agree with those of Hamady *et al.* [18] and Kuyper *et al.* [17] and show that the cells move to a downstream location in the boundary layer. When $\gamma = 3\pi/4$, the flow consists of a double convection cell. Similar to when $\gamma = \pi/2$, a stably stratified vertical temperature gradient exists in the interior of the enclosure. Both Hamady *et al.* [18] and Kuyper *et al.* [17] state that this is a conduction dominated flow. This is apparent from the fact that the flow is confined to the boundary layers with the heated and cooled fluid positioned in the upper and lower corners of the enclosure, respectively. When $\gamma = \pi/4$, the velocity at steady-state is nearly the maximum velocity. However, for $\gamma = \pi/2$ or $\gamma = 3\pi/4$, the velocity at steady-state is much less than the velocity during startup.

The time and length scales estimated from the velocity and temperature data are compared to those found using scale analysis in Table 1. The time and length scales estimated by scaling and experiment exhibit similar trends with the angle of inclination. As the apparent Rayleigh number decreases, the growth time of the thermal boundary layer increases and the velocity in the thermal boundary layer decreases. The experimental results for the intrusion layer also exhibit the trends predicted by scale analysis. An exception to this is the thickness scale for a viscous intrusion layer for $\gamma = 3\pi/4$. When $\gamma = 3\pi/4$, buoyancy and pressure oppose each other in the intrusion layer, and the order of magnitude assumptions made for the

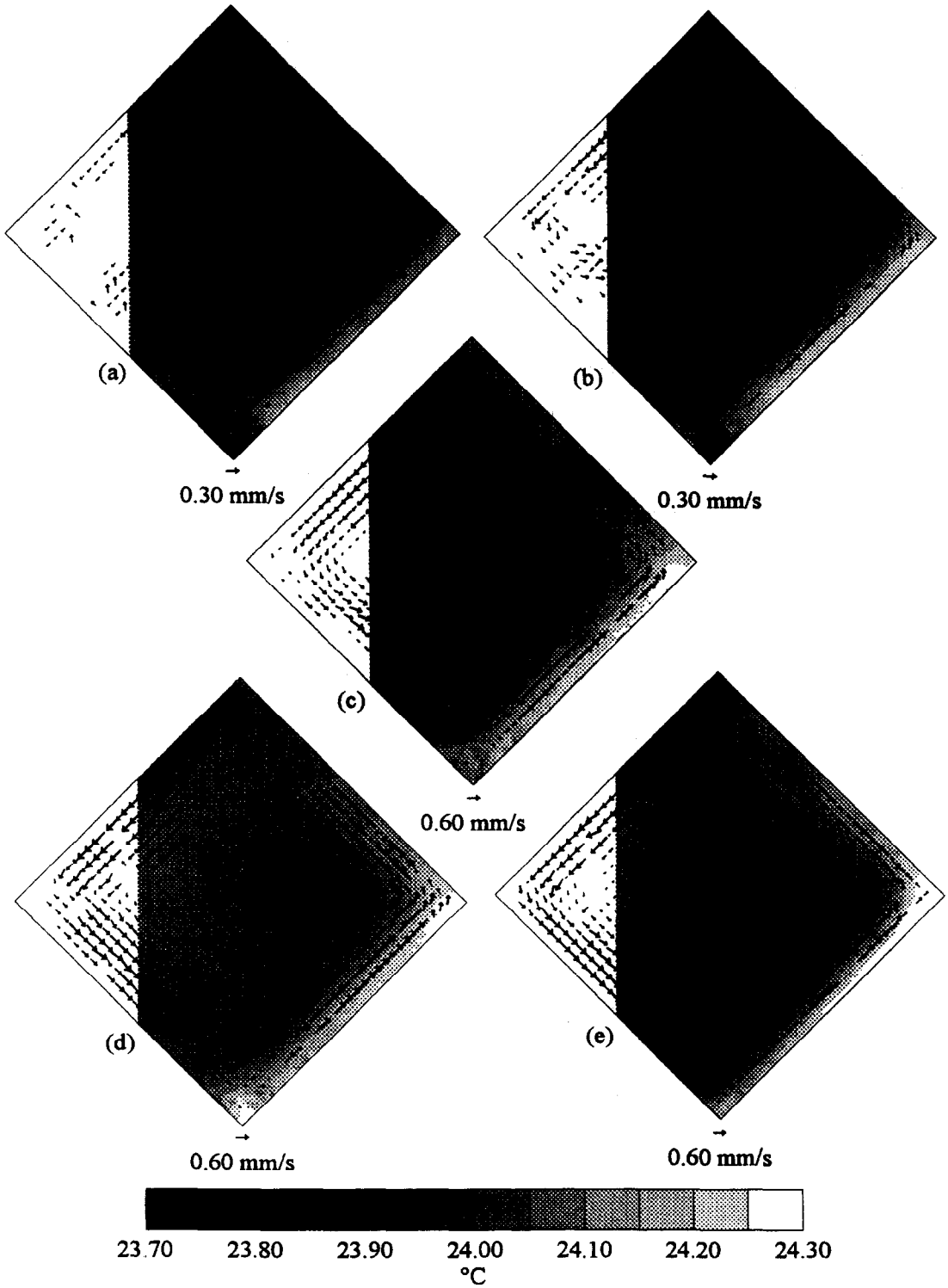

Fig. 4. Temperature and velocity fields during the evolution of the flow to steady-state for $\gamma = \pi/4$: (a) $t = 10$ s; (b) $t = 22$ s; (c) $t = 40$ s; (d) $t = 75$ s; (e) $t = 600$ s.

intrusion layer are no longer valid, since the pressure force is not small compared to the buoyancy force.

The temperature in the boundary layer and the Nusselt number at the wall and center of the enclosure as a function of time are shown for $\gamma = \pi/4$ in Fig. 7, $\gamma = \pi/2$ in Fig. 8 and $\gamma = 3\pi/4$ in Fig. 9. The temperature is normalized by $(T-T_0)/\Delta T$ and the locations in the boundary layer are normalized by $(x/W, y/H)$. The absence of data around 100 s occurs during data storage. The occurrence of either the two

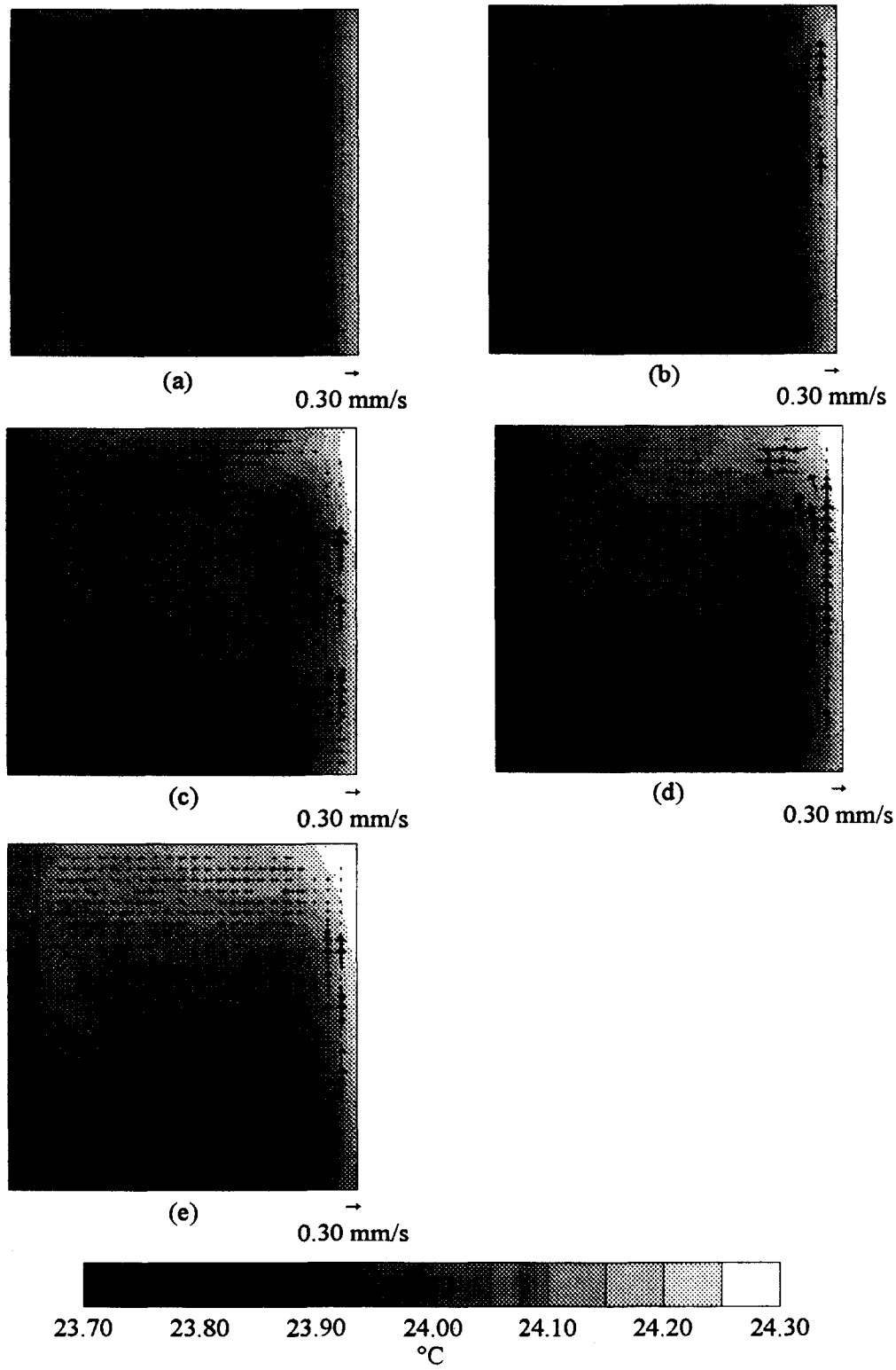

Fig. 5. Temperature and velocity fields during the evolution of the flow to steady-state for $\gamma = \pi/2$: (a) $t = 10$ s; (b) $t = 22$ s; (c) $t = 40$ s; (d) $t = 75$ s; (e) $t = 600$ s.

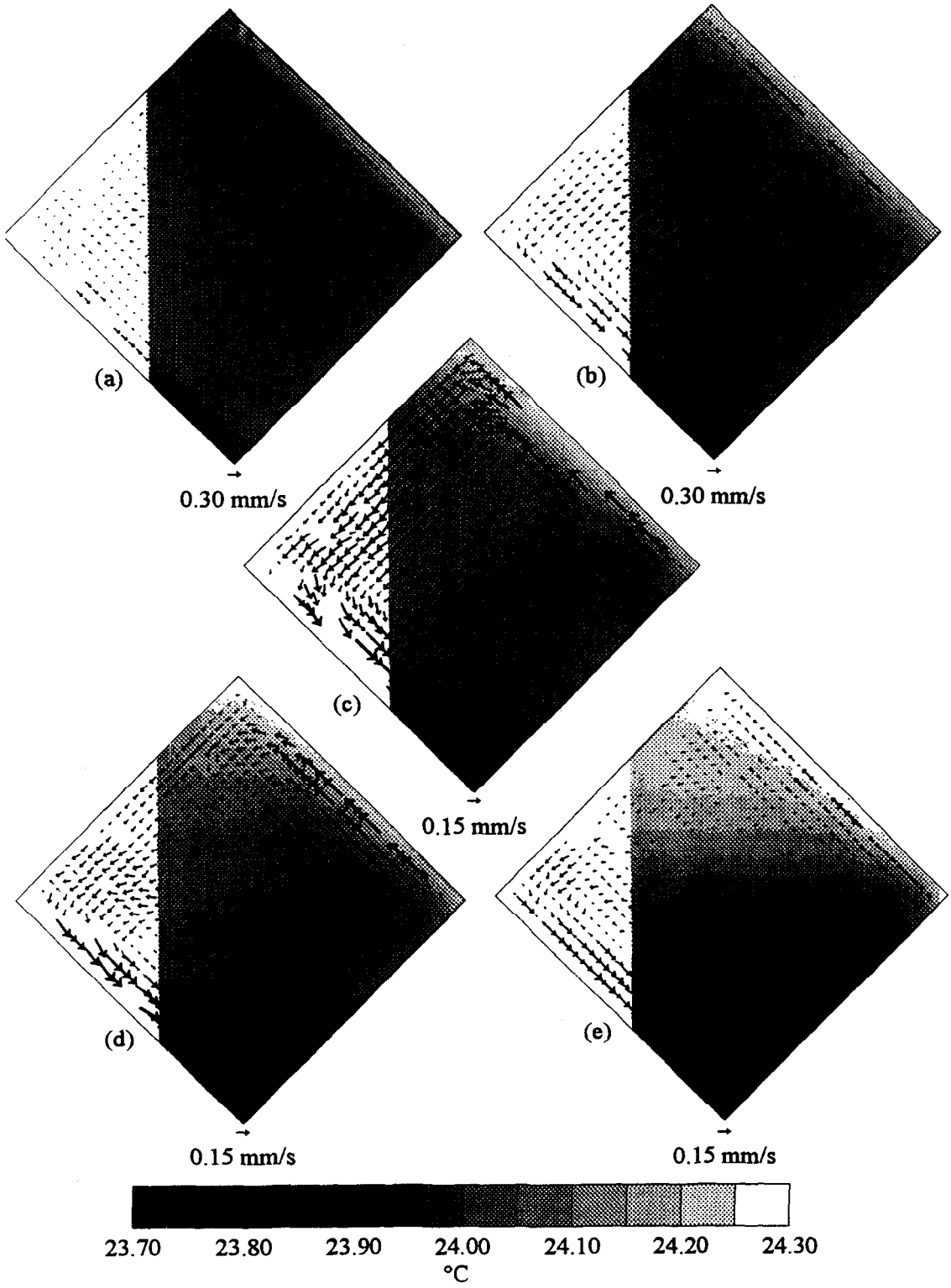

Fig. 6. Temperature and velocity fields during the evolution of the flow to steady-state for $\gamma = 3\pi/4$: (a) $t = 10$ s; (b) $t = 22$ s; (c) $t = 40$ s; (d) $t = 75$ s; (e) $t = 600$ s.

Table 1. Time and length scales estimated by scaling and experiment

Angle of inclination	Method	δ_T (mm)	τ (s)	v (mm/s)	δ_v (mm)	Δ_v (mm)	T_v (s)
$\gamma = \pi/4$	Scaling	1.7	19	1.5	4.2	1.7	19
	Experiment	4.0	22	0.4	6.4	5.8	34
$\gamma = \pi/2$	Scaling	1.5	16	1.8	3.9	3.2	34
	Experiment	3.9	18	0.6	6.4	9.4	38
$\gamma = 3\pi/4$	Scaling	1.7	19	1.5	4.2	1.7	19
	Experiment	3.7	22	0.4	6.4	12	36

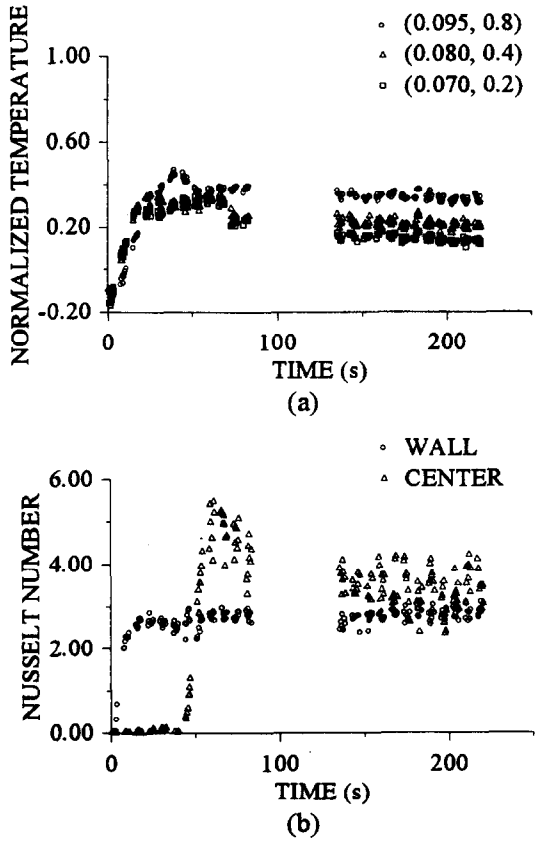

Fig. 7. (a) Temperature in the boundary layer; and (b) Nusselt number at the wall and center of the enclosure for $\gamma = \pi/4$.

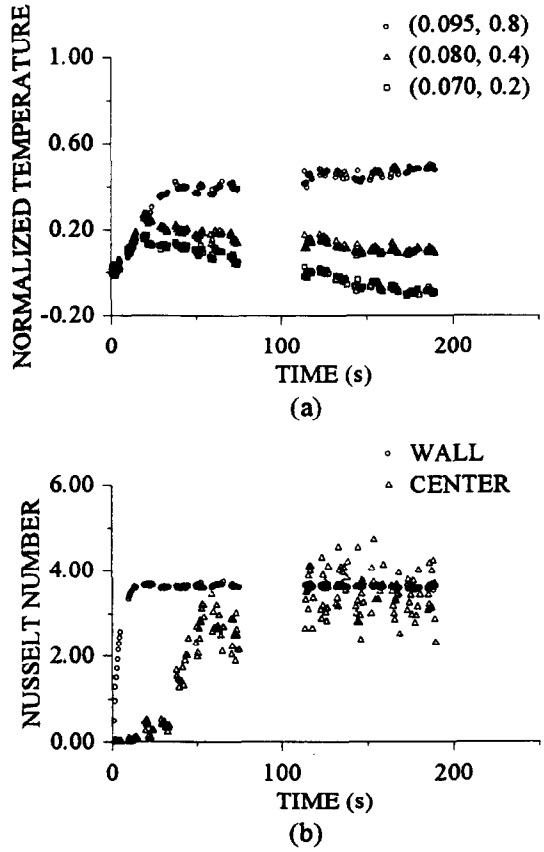

Fig. 8. (a) Temperature in the boundary layer; and (b) Nusselt number at the wall and center of the enclosure for $\gamma = \pi/2$.

boundary layer oscillations or the whole cavity oscillations is not clearly indicated. The period of the two boundary layer oscillations is $T = 27$ s and the period of the whole cavity oscillations is $T \sim 56$ s, so the time resolution is high enough to resolve both transient oscillations. There does appear to be an overshoot in the temperature in the boundary layer and a damped oscillation in the Nusselt number at the center of the enclosure for $\gamma = \pi/4$ as shown in Fig. 7, even though the uncertainty in the Nusselt number at the center of the enclosure is on the order of the magnitude of the oscillations [1, 3, 4]. A slight dip in the Nusselt number at the wall of the enclosure is also observed at the initiation of the damped oscillation. The current results for $\gamma = \pi/4$ are consistent with the numerical results Patterson and Imberger [1] made for a flow with $Pr = 7$, $Ra = 1.4 \times 10^4$, $A = 1.0$ and $\gamma = \pi/2$, in which they show a single damped oscillation. However, the temperature and velocity fields compare better with the results Patterson and Imberger [1] made for a flow with $Pr = 7$, $Ra = 1.4 \times 10^5$, $A = 1.0$ and $\gamma = \pi/2$. When $\gamma = \pi/4$, there is a rapid growth in

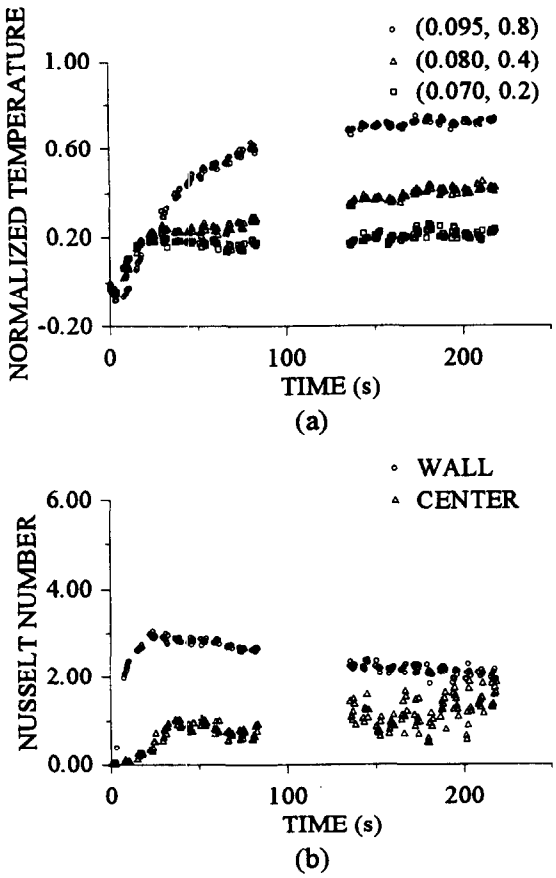

Fig. 9. (a) Temperature in the boundary layer; and (b) Nusselt number at the wall and center of the enclosure for $\gamma = 3\pi/4$.

the Nusselt number at the center of the enclosure, as the heated fluid crosses the enclosure. When $\gamma = \pi/2$, most of the fluid leaving the heated wall reaches the cooled wall. When $\gamma = 3\pi/4$, the flow is confined to the boundary layers and the Nusselt number grows slowly as the heat transfer is diffusion dominated.

Experimental considerations including fluid properties and boundary conditions may have affected the results. Differences in the fluid properties may have resulted from temperature variation and the addition of sodium bicarbonate. The temperature difference was 0.3°C and sodium bicarbonate was added to bring the density to 1.02×10^3 kg m^{-3}. Differences in the boundary conditions may have resulted from the finite time required to bring the heated and cooled walls to temperature, heat transfer through the adiabatic walls and the effect of the two end walls. The initiation time was 2.0 s, an order of magnitude less than the growth time scale of the boundary layer; the heat transfer through the adiabatic walls was negligible, evident in the temperature gradient normal to the adiabatic walls as shown in Figs. 4–6; and the length of enclosure was twice the height. These differences, especially the finite initiation time, may have a stabilizing effect on the flow.

7. CONCLUSIONS

The angle of inclination was shown to have a significant effect on the flow and heat transfer in natural convection in an enclosure. Buoyancy in the intrusion layer was found to be the main factor determining the character of these flows. The scale analysis for transient natural convection in enclosures was extended to inclined enclosures and compared to the experimental results. Neither the boundary layer nor the whole cavity transient oscillations were evident. The results for the temperature in the boundary layer and the Nusselt number at the wall and center of the enclosure have the appearance that they were produced by a lower Rayleigh number flow. This is probably due to differences in the boundary conditions at startup between the current experiments and the numerical simulations.

REFERENCES

1. Patterson, J. and Imberger, J., Unsteady natural convection in a rectangular cavity. *Journal of Fluid Mechanics*, 1980, **100**, 65–86.
2. Ivey, G. N., Experiments on transient natural convection in a cavity. *Journal of Fluid Mechanics*, 1984, **144**, 389–401.
3. Schladow, S. G., Oscillatory motion in a side-heated cavity. *Journal of Fluid Mechanics*, 1990, **213**, 589–610.
4. Patterson, J. C. and Armfield, S. W., Transient features of natural convection in a cavity. *Journal of Fluid Mechanics*, 1990, **219**, 469–497.
5. Armfield, S. W. and Patterson, J. C., Wave properties of natural-convection boundary layers. *Journal of Fluid Mechanics*, 1992, **239**, 195–211.
6. Briggs, D. G. and Jones, D. N., Two-dimensional periodic natural convection in a rectangular enclosure of aspect ratio one. *Journal of Heat Transfer*, 1985, **107**, 850–854.
7. Winters, K. H., Hopf bifurcation in the double-glazing problem with conducting boundaries. *Journal of Heat Transfer*, 1987, **109**, 894–898.
8. Gebhart, B. and Mahajan, R. L., Instability and transition in buoyancy induced flows. *Advances in Applied Mechanics*, 1982, **22**, 231–315.
9. Hieber, C. A. and Gebhart, B., Stability of vertical natural convection boundary layers: some numerical solutions. *Journal of Fluid Mechanics*, 1971, **48**, 625–646.
10. Bejan, A., *Convection Heat Transfer*, 2nd end. John Wiley, New York 1995, pp. 18–21, 194–196, 219–267.
11. Upton, T. D. and Watt, D. W., Calibrated multichannel electronic interferometry for quantitative flow visualization. *Experiments in Fluids*, 1993, **14**, 271–276.
12. Upton, T. D. and Watt, D. W., Optical and electronic design of a calibrated multichannel electronic interferometer for quantitative flow visualization. *Applied Optics*, 1995, **34**, 5602–5610.
13. Willert, C. E. and Gharib, M., Digital particle image velocimetry. *Experiments in Fluids*, 1991, **10**, 181–193.
14. Vest, C. M., *Holographic Interferometry*, 1st edn. John Wiley, New York, 1979, pp. 329–334.
15. Holman, J. P., *Experimental Methods for Engineers*, 5th edn. McGraw-Hill, New York, 1989, pp. 41–47.
16. Upton, T. D., Experiments on transient natural convection in inclined enclosures using calibrated multi-

channel electronic interferometry and digital particle image velocimetry. Ph.D. thesis, University of New Hampshire, Durham, New Hampshire, 1995.
17. Kuyper, R. A., van der Meer, TH. H., Hoogendoorn, C. J., and Henkes, R. A. W. M., Numerical study of laminar and turbulent natural convection in an inclined square cavity. *International Journal of Heat and Mass Transfer*, 1993, **36**, 2899–2911.
18. Hamady, F. J., Lloyd, J. R., Yang, H. Q. and Yang, K. T., Study of local natural convection heat transfer in an inclined enclosure. *International Journal of Heat and Mass Transfer*, 1989, **32**, 1697–1708.